

Control of Geometric Phase by Dynamic Phase

Aleksi Leinonen^{1,2,*} Taco D. Visser^{3,4,5} Ari T. Friberg,¹ and Tommi K. Hakala^{1,†}


¹*Center for Photonics Sciences, University of Eastern Finland, P.O. Box 111, FI-80101 Joensuu, Finland*

²*VTT Technical Research Centre of Finland, P.O. Box 1100, FI-90571 Oulu, Finland*

³*Department of Physics and Astronomy, Vrije Universiteit, 1081 HV Amsterdam, Netherlands*

⁴*The Institute of Optics, University of Rochester, Rochester, New York 14627, USA*

⁵*School of Physics and Electronics, Shandong Normal University, Jinan 250358, China*

 (Received 28 February 2023; revised 21 December 2023; accepted 22 December 2023; published 18 January 2024)

The geometric and dynamic phases are generally treated as independent and together give rise to the total phase of a system. Here, we present a scenario in which these two phases become strongly interdependent. We achieve this by introducing a modified Young's double-slit configuration that supports surface plasmon polaritons (SPPs) propagating between the slits. Remarkably, by varying the slit separation distance, and hence the dynamic SPP phase, by just a single plasmon wavelength, the geometric phase can be significantly modified.

DOI: [10.1103/PhysRevApplied.21.014033](https://doi.org/10.1103/PhysRevApplied.21.014033)

I. INTRODUCTION

The phase of a physical system is the sum of two contributions, a dynamic phase and a geometric phase. The first evolves with time, whereas the second is accrued when the system is made to trace out a (usually closed) path. Geometric phases can be divided into four groups. The system can either be a classical system or a quantum system, and the trajectory that is taken can be in real space or in some abstract parameter space [1,2]. For example, Foucault's pendulum is a classical system that travels through real space [3]. The Pancharatnam phase that appears in polarized light beams pertains to a classical system that is moved across the parametric Poincaré sphere [4,5]. The Berry phase describes quantum systems with a Hamiltonian that undergoes a cyclical change of its parameters [6]. An example of the fourth variety is the Aharonov-Bohm effect [7]. In optics the Pancharatnam-Berry (PB) geometric phase accumulates when the polarization state of an electromagnetic field undergoes a series of in-phase changes [4] that form a closed polarization-state path on the Poincaré sphere. Each polarization state is represented by a point on the sphere [8], and the geometric phase is then given by half the solid angle subtended by the polarization path [4]. The total phase of the system is the sum of the geometric and the accumulated dynamic phase, the latter being associated with the propagation of the electromagnetic wave. The geometric phase can therefore be accessed by separating or eliminating the dynamic phase.

For example, in a quantum system a static magnetic field may be employed to eliminate the dynamic phase with no effect on the geometric phase [9].

Typically, the geometric phase in optics has been measured with a Mach-Zehnder setup [10,11] by keeping the dynamic phase constant and adjusting only the geometric phase via changes of the polarization state [12,13]. In previous work, we have pioneered studies of the geometric phase in Young's double-slit arrangement [14–16]. In those studies moving the far-zone point of observation transports the state of polarization on the Poincaré sphere. The geometric phase can be controlled by adjusting the input-field intensities and polarizations. However, the dynamic phases of the input fields have no effect on the acquired geometric phase.

The presence of surface plasmon polaritons (SPPs) [17,18] profoundly alters light transmission in Young's experiment [19–21], because they establish a polarization-specific coupling mechanism between the slit fields. SPPs are fully polarized and completely coherent, with a well-defined phase. In traveling between the two slits, the polarization state of the SPPs does not change and thus they only acquire a dynamic phase.

In this paper, we introduce a scenario in which tailoring the dynamic SPP phase gives precise control over the geometric phase of the far-zone field. We identify four specific cases, in which (1) the presence of SPPs has no effect on the acquired PB phase, (2) SPPs induce a PB phase which is independent of the plasmon travel distance and hence its dynamic phase, (3) SPPs create a propagation-distance-dependent PB phase, and (4) the range of the PB phase variation depends on the SPP travel distance as well

*aleksi.leinonen@vtt.fi

†tommi.hakala@uef.fi

as on the plasmonic [transverse magnetic (TM)] and non-plasmonic [transverse electric (TE)] input fields. We find that the PB phase can change continuously over almost the full range $-\pi$ to π , and that virtually the whole Poincaré sphere can be covered, when the plasmon propagation distance between the slits is varied by only a single SPP wavelength.

II. THEORY

We employ an intuitive, phenomenological model [19, 20] to describe the fields emanating from a metallic Young's double-slit arrangement (see Fig. 1). The model treats the slits as line sources that radiate cylindrical waves. The field contributions in the model are divided into s -polarized (TE) and p -polarized (TM) incident fields that are transmitted through the slits. In addition to the transmitted field, the p -polarized field also induces an SPP field which propagates a distance a from one slit to the other and then partially scatters to the far field. The output fields are described with complex coefficients corresponding to p -polarized transmission (α), s -polarized transmission (β), scattered SPPs (γ), and a plasmon propagation factor $K = \exp(ik_{\text{sp}}a)$ [20]. Here, k_{sp} is the SPP wave vector given by the expression $k_{\text{sp}} = (\omega/c)n_m/(1+n_m^2)^{1/2}$ [17], where n_m is the metal's complex refractive index at frequency ω . The slit separation a is chosen such that it is less than the SPP decay length $l_{\text{sp}} = 1/\text{Im}(k_{\text{sp}})$ (where Im denotes the imaginary part), and that SPP reflections may be neglected. The complex output fields for slit $u = 1, 2$ then become

$$\mathbf{E}_u = \begin{bmatrix} E_{xu} \\ E_{yu} \end{bmatrix} = \begin{bmatrix} \alpha E_{pu} + \gamma K E_{pv} \\ \beta E_{su} \end{bmatrix}, \quad (1)$$

where $v = 2, 1$ is the other slit, E_{xu} and E_{yu} are the p - and s -polarized field components at the output, and similarly, E_{pu} and E_{su} are the electric field components at the input of the slit, respectively.

In the system considered, a monochromatic ($\lambda = 800$ nm) plane wave \mathbf{E}_{in} is incident on a 200-nm-thick silver screen ($n_m = 0.280 + i5.630$ [22]) with two 250-nm-wide slits. A 20-nm Ti layer suppresses plasmons on the input

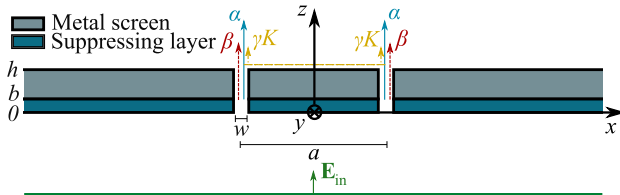


FIG. 1. Schematic of a metallic Young's double-slit setup with associated model coefficients α , β , and γK . The parameters are: height of the structure h , suppressing layer thickness b , slit separation a , and slit width w . The medium above the metal is air and \mathbf{E}_{in} denotes the incident electric field.

side. We employ a well-established Fourier modal method (FMM) to rigorously solve Maxwell's equations for this geometry [20,23], detailed in Appendix A. The coefficients determined from the FMM are $\alpha = -0.026 - i0.499$, $\beta = -0.1189 + i0.210$, and $\gamma = -0.065 + i0.082$, with $k_{\text{sp}} = 7.980 + i0.012$. This corresponds to an SPP wavelength of $\lambda_{\text{sp}} = 2\pi/\text{Re}(k_{\text{sp}}) \approx 787$ nm (where Re denotes the real part). The validity of this model has been demonstrated experimentally [19]. Furthermore, rigorous comparison with FMM results confirms that our phenomenological model is accurate for slit separations exceeding $a \approx 10 \lambda_{\text{sp}}$ [20]. The polarization states are described with the help of Stokes parameters [24]

$$S_{0u} = |E_{xu}|^2 + |E_{yu}|^2, \quad (2a)$$

$$S_{1u} = |E_{xu}|^2 - |E_{yu}|^2, \quad (2b)$$

$$S_{2u} = 2 \text{Re}(E_{xu}^* E_{yu}), \quad (2c)$$

$$S_{3u} = 2 \text{Im}(E_{xu}^* E_{yu}), \quad (2d)$$

where the output field components (E_{xu}, E_{yu}), $u = 1, 2$, are given in accordance with Eq. (1).

We analyze plasmon propagation effects with the slit separation a being varied over a single SPP wavelength. Within this range, the travel losses are negligible as the SPP intensity decays by less than a factor of 2×10^{-4} . When the plasmon travel distance $a = N \lambda_{\text{sp}}$ is increased to $a = (N + \frac{1}{2}) \lambda_{\text{sp}}$, with N an integer, the propagation factor K is multiplied by $\exp(i\pi)$ and changes sign. Thus (in these extreme cases), either destructive ($+K$) or constructive ($-K$) interference between the SPP-converted (γK) and the directly transmitted (α) fields is obtained [19]. The maximum transmittance appearing at $(N + \frac{1}{2}) \lambda_{\text{sp}}$ may seem counterintuitive, but it is consistent with the Huygens-Fresnel principle [25] in light-SPP-light scattering.

In Young's double-slit arrangement the magnitude of the PB phase is given by the intensities and the Stokes parameters at the two slits as [14]

$$|\Phi_{\text{PB}}| = \pi - \pi \frac{|S_{01} - S_{02}|}{|\mathbf{P}_1 - \mathbf{P}_2|}, \quad (3)$$

where $\mathbf{P}_u = S_{1u} \hat{s}_1 + S_{2u} \hat{s}_2 + S_{3u} \hat{s}_3$ is the Poincaré vector for slit u and Φ_{PB} is positive if the path on the Poincaré sphere taken by moving the observation point is traversed counterclockwise ($S_{01}/S_{02} < 1$; see Eq. (21) in [14]). Near the limit $S_{01} \approx S_{02}$ the polarization path is a great circle. With $S_{01}/S_{02} > 1$ the direction is clockwise, resulting in a negative PB phase. The correctness of Eq. (3) has been proven numerically and experimentally [14–16].

According to Eq. (3), we need to have some asymmetry between the output fields at the two slits in order to have a nonzero Φ_{PB} . This asymmetry can either be at the polarization or at the phase level, as we will next explore.

III. POLARIZATION ASYMMETRY

To introduce asymmetry to the system at the polarization level we first consider perpendicular incident-field polarization states, namely, an s -polarized input for slit 1 ($E_{s1} = 1$) and a p -polarized input for slit 2 ($E_{p2} = 1$). Thus, SPPs will be generated only at slit 2, which propagate to slit 1 and can there scatter to the far field. In such a situation it is expected that both the intensity S_{01} and the Poincaré vector \mathbf{P}_1 will be affected by the slit distance a . A natural question now arises: is the resulting PB phase dependent on a ?

The output electric fields for slit 1 are $E_{x1} = \gamma K$ and $E_{y1} = \beta$, whereas for slit 2 they are $E_{x2} = \alpha$ and $E_{y2} = 0$. The Stokes parameters for slit 1 become

$$S_{01} = |\gamma K|^2 + |\beta|^2, \quad (4a)$$

$$S_{11} = |\gamma K|^2 - |\beta|^2, \quad (4b)$$

$$S_{21} = 2 \operatorname{Re}[(\gamma K)^* \beta], \quad (4c)$$

$$S_{31} = 2 \operatorname{Im}[(\gamma K)^* \beta]. \quad (4d)$$

For slit 2 they are $S_{02} = S_{12} = |\alpha|^2$ and $S_{22} = S_{32} = 0$. From Eq. (3) and the expressions for S_{01} and S_{02} above we find that the sign change of K only influences the denominator in Eq. (3), which is

$$|\mathbf{P}_1 - \mathbf{P}_2| = [(\Delta S_1)^2 + (\Delta S_2)^2 + (\Delta S_3)^2]^{1/2}, \quad (5)$$

where $\Delta S_m = S_{m1} - S_{m2}$, $m = 1, 2, 3$, are the Stokes parameter differences. The quantity ΔS_1 involves the absolute value $|K|$, hence the denominator becomes

$$|\mathbf{P}_1 - \mathbf{P}_2| = [(\Delta S_1)^2 + 4|\beta|^2|\gamma K|^2]^{1/2}. \quad (6)$$

Importantly, again only the absolute value $|K|$ shows up, implying that the dynamic phase of SPPs has no effect on the system response.

Figure 2 illustrates the polarization-state paths determined from the far-field intensity patterns (see Appendix B for formulas), when the slit separation is varied between (blue) constructive $a = 10.38 \lambda_{\text{sp}}$ (red) and destructive $a = 10.84 \lambda_{\text{sp}}$ (yellow) interference. We note that the polarization paths are circles on the Poincaré sphere, similar to the nonplasmonic two-beam case [15], resulting in a nonzero PB phase. However, the plasmonic influence only tilts the polarization paths with no change in the PB phase magnitude. These results suggest that while with perpendicular input polarizations the SPP travel distance a does affect the path taken on the Poincaré sphere, the solid angle, and therefore the PB phase, remains constant.

We now add an s -polarized component to the input of slit 2 ($E_{s2} = 1$). As s -polarized light cannot excite SPPs, one might expect that this will not affect the SPP-induced PB

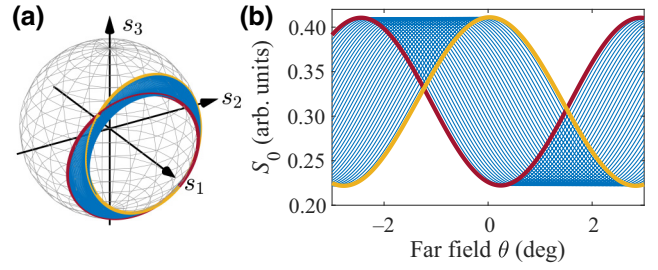


FIG. 2. Polarization paths and interference patterns for input-field components $E_{1p} = E_{2s} = 0$ and $E_{1s} = E_{2p} = 1$, without PB phase modulation. (a) Polarization paths on the Poincaré sphere presented using normalized Stokes parameters, and (b) the corresponding far-field intensity patterns. The yellow line (light gray) depicts constructive interference ($a = 10.38 \lambda_{\text{sp}}$), the red line (dark gray) destructive interference ($a = 10.84 \lambda_{\text{sp}}$), and blue (gray) lines depict cases in between.

phase. However, it introduces changes in all slit 2 Stokes parameters, which become

$$S_{02} = |\alpha|^2 + |\beta|^2, \quad (7a)$$

$$S_{12} = |\alpha|^2 - |\beta|^2, \quad (7b)$$

$$S_{22} = 2 \operatorname{Re}(\alpha^* \beta), \quad (7c)$$

$$S_{32} = 2 \operatorname{Im}(\alpha^* \beta). \quad (7d)$$

For slit 1 the parameters are given by Eq. (4). Again, $\Delta S_0 = S_{01} - S_{02}$, which is the numerator in Eq. (3), and ΔS_1 make no contribution to the PB phase modulation. The denominator in Eq. (3) takes the form

$$|\mathbf{P}_1 - \mathbf{P}_2| = \{(\Delta S_1)^2 + 4|\beta|^2[|\alpha|^2 + |\gamma K|^2 - 2 \operatorname{Re}(\alpha \gamma^* K^*)]\}^{1/2}. \quad (8)$$

Here, the last term that involves γK has important implications. In contrast to the previous case, the propagation factor K and thus the dynamic phase of the SPPs now contributes to the modulation of the PB phase. Intriguingly, the nonplasmonic term α (with no influence on SPP field strength) appears as a factor in the last term. This indicates also that the strength of the nonplasmonic field is crucial for the plasmonic PB phase. The different polarization paths are illustrated in Fig. 3(a), where the magnitude of the PB phase varies between $|\Phi_{\text{PB}}| = 0.22\pi$ and $|\Phi_{\text{PB}}| = 0.35\pi$, corresponding respectively to constructive ($a = 10.38 \lambda_{\text{sp}}$) and destructive ($a = 10.84 \lambda_{\text{sp}}$) interference.

If, instead of adding s -polarized light to slit 2, we add a p -polarized field to slit 1, results almost similar to Eq. (8) are obtained but the sign of the modulating real part changes, as detailed in Appendix C. Consequently, constructive interference ($-K$) increases the magnitude of the PB phase while destructive interference ($+K$) decreases it. However, the range of the modulation remains the same.

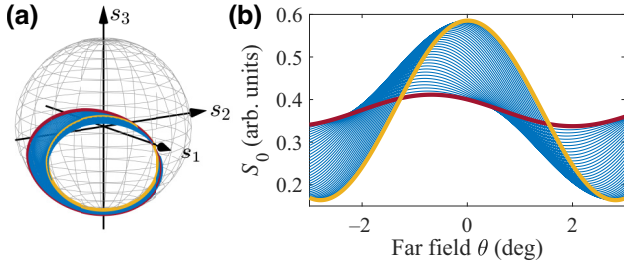


FIG. 3. Polarization paths and interference patterns for input-field components $E_{1p} = 0$ and $E_{1s} = E_{2p} = E_{2s} = 1$, with PB phase modulation. (a) Polarization paths on the Poincaré sphere presented using normalized Stokes parameters, and (b) the corresponding far-field intensity patterns. The yellow line (light gray) depicts constructive interference ($a = 10.38 \lambda_{\text{sp}}$), the red line (dark gray) destructive interference ($a = 10.84 \lambda_{\text{sp}}$), and blue (gray) lines depict cases in between.

To summarize the above findings, we have identified three cases where SPPs show significantly different effects on the PB phase. First, they have no influence if the input-field polarizations are equal. Second, they will induce a constant, propagation-independent PB phase if orthogonal (p and s) input polarizations are applied. This case is intriguing, as the polarization trajectory encloses a finite area on the Poincaré sphere and the SPP travel distance also modifies the path taken on the sphere. However, fulfilling these two prerequisites is not a sufficient condition for PB phase modulation, since the area enclosed on the Poincaré sphere remains constant. Third, and surprisingly, an SPP propagation-dependent PB phase can be achieved by adding a nonplasmonic (s -polarized) field to one of the inputs. This last case is of interest as one might assume that SPP-induced modulation is only related to the strength of the plasmons and not to the transmitted nonplasmonic fields. Thus, a nonplasmonic field is essential for the emergence of the SPP-mediated PB phase effects. These results are unique for the present SPP-coupled double-slit system, as the conventional setup has no intermixing between the slits ($\gamma K = 0$).

IV. PHASE ASYMMETRY

The range of phase modulation achievable with SPPs will be essential for any practical implementation. Therefore, we study a generic case by allowing both plasmonic and nonplasmonic fields to enter each slit with arbitrary relative phases. The fields in slit 1 are $E_{p1} = 1$ and $E_{s1} = B$ and likewise in slit 2 $E_{p2} = A$ and $E_{s2} = 1$, where A and B are unit-amplitude fields ($|A| = |B| = 1$) of phases ϕ_A and ϕ_B . The corresponding output fields then become

$$\mathbf{E}_1 = \begin{bmatrix} \alpha + \gamma K A \\ \beta B \end{bmatrix}, \quad \mathbf{E}_2 = \begin{bmatrix} \alpha A + \gamma K \\ \beta \end{bmatrix}. \quad (9)$$

Applying these output fields to Eqs. (2), the Stokes parameter differences assume the form

$$\Delta S_0 = \Delta S_1 = 4 \operatorname{Re}[i\alpha^* \gamma K \sin(\phi_A)], \quad (10a)$$

$$\Delta S_2 = 2 \operatorname{Re}[\beta(\alpha^*[\exp(i\phi_B) - \exp(-i\phi_A)] + \gamma^* K^* \{\exp[i(\phi_B - \phi_A)] - 1\})], \quad (10b)$$

$$\Delta S_3 = 2 \operatorname{Im}[\beta(\alpha^*[\exp(i\phi_B) - \exp(-i\phi_A)] + \gamma^* K^* \{\exp[i(\phi_B - \phi_A)] - 1\})], \quad (10c)$$

where ΔS_0 [the numerator in Eq. (3)] now has a plasmonic contribution (γK). In addition, the phase of the nonplasmonic contribution ϕ_B has a major influence on the plasmonic terms (γK).

To maximize the plasmonic influence, setting $\phi_A = \pi/2$ appears as a plausible choice, since then the sine factor in Eq. (10a) becomes unity. Intriguingly, this also gives us two options: we can maximize the plasmonic modulation in the second and the third Stokes parameter differences [Eqs. (10b) and (10c)] by taking $\phi_B = -\phi_A$, or minimize it with $\phi_B = \phi_A$. The first choice removes the nonplasmonic term (α) and maximizes the plasmonic terms (γK), whereas the second choice makes the plasmonic term vanish and maximizes the nonplasmonic contribution. When other values for ϕ_A are considered we find that the maxima and minima of the plasmonic modulation are found when $\phi_B - \phi_A = n\pi$, where n is an integer. The maximum plasmonic influence is achieved with odd n , while even n gives the minimum. The nonplasmonic term on the other hand vanishes only when $\phi_B = \phi_A$, meaning that the plausible choice ($\phi_A = \pi/2$) is a special case with the highest plasmonic influence in this configuration.

Figure 4(a) illustrates the achievable range of variation over a single plasmon wavelength, when $\phi_A = \pi/2$ and the PB phases are numerically determined over a range $\phi_B = (0, 2\pi)$ starting from $a = 10.1 \lambda_{\text{sp}}$. The blue region, limited by extreme cases, gives all the values of a with a 1-nm interval. Notably, the extrema provide the range of all possible values for Φ_{PB} and form a kind of forbidden zone at the center (white region). On the other hand, the intermediate cases constitute a plateau around the maximum plasmonic influence ($\phi_B = 3\pi/2$) that resembles a bandgap.

Figure 4(b) demonstrates how the acquired PB phase is an extremely sensitive function of the plasmon propagation distance. With a choice of $\phi_B = 3\pi/2$, virtually all values from $-\pi$ to π can be covered by varying the SPP propagation distance by only one SPP wavelength. This feature could be highly beneficial for various sensing applications, as minor changes of the refractive index at the dielectric-metal interface are expected to result in similar variation of the PB phase.

Figure 4(c) shows the corresponding polarization-state paths on the Poincaré sphere. Intriguingly, we find two

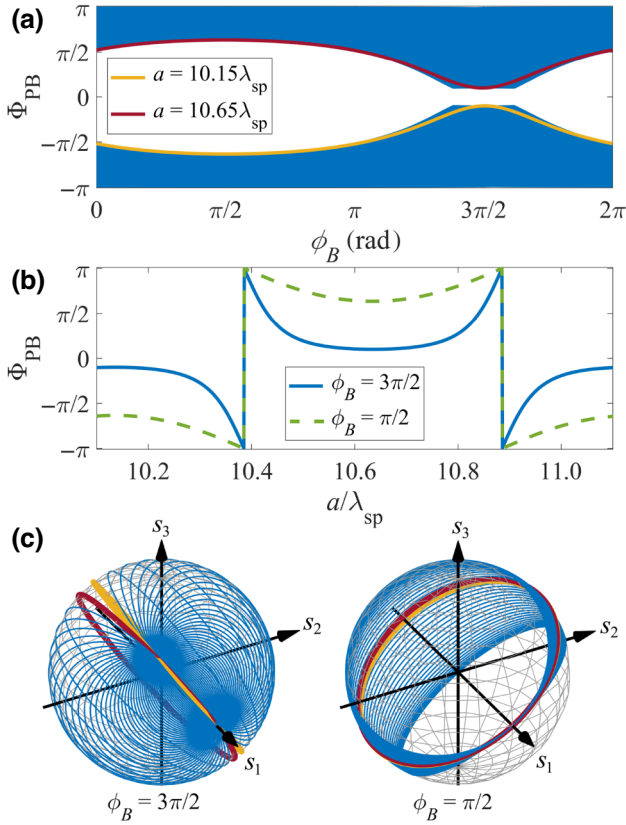


FIG. 4. Range of PB phase modulation with phase asymmetry. (a) Phase ϕ_B is varied to determine the modulation range for Φ_{PB} with $\phi_A = \pi/2$ and plasmon propagation distances of $10.1 \lambda_{sp} \leq a \leq 11.1 \lambda_{sp}$. The blue (gray) lines give all possible Φ_{PB} of the range for a ; constructive interference is shown by the red (black) line and destructive by the yellow (light gray) line. (b) The maximum (solid blue) and minimum (dashed green) range of Φ_{PB} modulation when distance a is varied over a single plasmon wavelength λ_{sp} . (c) Polarization paths presented using normalized Stokes parameters for the cases in (b), where the paths near the limit of $B = A$ are shown with red (black) and yellow (light gray) lines and all other paths with blue (gray) lines.

points on the sphere, through which all the polarization paths pass. One point is at the center of the geodesic connecting the two slit polarization states, and the other is the fully p -polarized point. By further optimization of the system parameters (increasing the p -polarized intensities), these two points can be made to approach each other, allowing virtually the whole range of $\pm\pi$ and thus the entire Poincaré sphere to be covered by varying the plasmon propagation distance by only one SPP wavelength.

V. CONCLUSIONS

We have put forward a scenario in which the geometric phase, usually detached from the dynamic phase, can be controlled by the propagation-dependent dynamic phase. This is achieved in a modified Young's two-slit

arrangement supporting SPPs, which could be experimentally realized by a setup based on a digital micromirror device [15,16] where a wedge-shaped structure with two coherently illuminated grooves provides the variation in slit separation [26]. Our theoretical results exploit previous numerical and experimental research which have verified that the physical model is accurate for the present setup. Four specific cases were identified, ranging from no plasmon-induced effects to a case where SPP propagation over a single plasmon wavelength can modulate the acquired PB phase virtually continuously from $-\pi$ to $+\pi$. The polarization paths can cover almost the whole Poincaré sphere, allowing unprecedented control of the polarization state by minor changes in the dynamic phase. Our results may be beneficial in improving the performance of metasurfaces [27–29] and in various other applications ranging from refractive index sensing to novel PB geometric-phase active optical elements. On a more general level, our findings constitute a paradigm shift toward precise control of the geometric phase via very small changes in the dynamic phase. Whether our results could be generalized to other classical and quantum mechanical systems remains an interesting prospect for future studies.

ACKNOWLEDGMENT

This work is part of the Research Council of Finland's flagship program Photonics Research and Innovation (PREIN, 346518), and project numbers 322002 and 359450. AL thanks the Finnish Cultural Foundation for financial support. TDV acknowledges support from the Joensuu University Foundation.

APPENDIX A: FOURIER MODAL METHOD CALCULATIONS

The Fourier modal method (FMM) is a rigorous calculation technique, where the monochromatic fields in the defined periodic system are calculated in the frequency domain [23]. Aperiodic systems can be simulated with FMM by utilizing perfectly matched layers (PMLs) and coordinate transforms or by using a period that is sufficiently large to be considered aperiodic. In our implementation of the FMM we use an S-matrix formulation, where we apply a coordinate transform to the edges of the system and gradually apply the PMLs to both sides. The width of coordinate transform on a single side was set as $8 \mu\text{m}$ and $20 \mu\text{m}$ was used for a single PML.

We used the FMM to calculate the coefficients for our system, where the width of the computational period was set to $160 \mu\text{m}$, the height of the silver screen was 200 nm , and the thickness of the suppressing layer of Ti was 20 nm . The refractive indices were taken from Ref. [22] for 800-nm incident light. For an accurate representation of the defined system the FMM requires a sufficient number of truncation orders for the calculations to converge. The

convergence was verified for our system by calculating the efficiencies of the ± 1 st diffraction orders over a number of truncation orders. The system was deemed to be accurate with 1200 orders, but we nevertheless used 2500 orders. The coefficients were calculated as discussed in Ref. [20]. In order to avoid the effects of SPP propagation in γ we averaged over a distance of $2\lambda_{\text{sp}}$ from the plasmon decay length of $80.51\ \mu\text{m}$ to $82.17\ \mu\text{m}$.

APPENDIX B: FAR-FIELD INTERFERENCE PATTERNS

The Stokes parameters in the paraxial far field are calculated by utilizing the polarization matrix [24]

$$\mathbf{J} = \begin{bmatrix} J_{xx} & J_{xy} \\ J_{yx} & J_{yy} \end{bmatrix}, \quad (\text{B1})$$

where $J_{cd} = \langle E_c^* E_d \rangle$ with c, d corresponding to an either p -polarized (x) or s -polarized (y) field. Using the polarization matrix presentation, the Stokes parameters at a far-field angle θ are

$$S_0(\theta) = J_{xx}(\theta) + J_{yy}(\theta), \quad (\text{B2})$$

$$S_1(\theta) = J_{xx}(\theta) - J_{yy}(\theta), \quad (\text{B3})$$

$$S_2(\theta) = J_{xy}(\theta) + J_{yx}(\theta), \quad (\text{B4})$$

$$S_3(\theta) = i[J_{yx}(\theta) - J_{xy}(\theta)], \quad (\text{B5})$$

where S_0 is the intensity pattern. To obtain the polarization trajectories from the far-field interference pattern we formally take the two slits as line sources and use the angular spectrum method on the model fields [Eq. (1) of the main text] as detailed in Appendix A of [20]. For the elements of the polarization matrix we then get a rather involved form:

$$\begin{aligned} J_{xx}(\theta) &= |\alpha E_{p1} + \gamma K E_{p2}|^2 + |\alpha E_{p2} + \gamma K E_{p1}|^2 \\ &\quad + 2 \operatorname{Re}[(\alpha E_{p1} + \gamma K E_{p2})^* (\alpha E_{p2} + \gamma K E_{p1})] \\ &\quad \times \exp(-ik_0 a \sin \theta), \end{aligned} \quad (\text{B6})$$

$$\begin{aligned} J_{xy}(\theta) &= \beta E_{s1} (\alpha E_{p1} + \gamma K E_{p2})^* \\ &\quad + \beta E_{s2} (\alpha E_{p2} + \gamma K E_{p1})^* \\ &\quad + \beta E_{s2} (\alpha E_{p1} + \gamma K E_{p2})^* \exp(-ik_0 a \sin \theta) \\ &\quad + \beta E_{s1} (\alpha E_{p2} + \gamma K E_{p1})^* \exp(ik_0 a \sin \theta), \end{aligned} \quad (\text{B7})$$

$$\begin{aligned} J_{yx}(\theta) &= \beta^* E_{s1}^* (\alpha E_{p1} + \gamma K E_{p2}) \\ &\quad + \beta^* E_{s2}^* (\alpha E_{p2} + \gamma K E_{p1}) \\ &\quad + \beta^* E_{s1}^* (\alpha E_{p2} + \gamma K E_{p1}) \exp(-ik_0 a \sin \theta) \\ &\quad + \beta^* E_{s2}^* (\alpha E_{p1} + \gamma K E_{p2}) \exp(ik_0 a \sin \theta), \end{aligned} \quad (\text{B8})$$

$$\begin{aligned} J_{yy}(\theta) &= |\beta E_{s1}|^2 + |\beta E_{s2}|^2 \\ &\quad + 2|\beta|^2 \operatorname{Re}[E_{s1}^* E_{s2} \exp(-ik_0 a \sin \theta)]. \end{aligned} \quad (\text{B9})$$

Next, the Stokes parameters are calculated with Eqs. (B2)–(B5). These formulas can now be used to plot

the polarization paths for every case with any input field or coefficient value by restricting the far-field angle to match a single period.

APPENDIX C: POLARIZATION-LEVEL ASYMMETRY

In this case both p -polarized and s -polarized light is added to slit 1 ($E_{p1} = 1, E_{s1} = 1$) and only p -polarized light to slit 2 ($E_{p2} = 1, E_{s2} = 0$) to maintain polarization-level asymmetry. The p -polarized fields at the slits are identical: $E_{x1} = E_{x2} = \alpha + \gamma K$. As with previous cases, only the second and third Stokes parameters affect the modulation of PB phase via the denominator, which becomes

$$\begin{aligned} |\mathbf{P}_1 - \mathbf{P}_2| &= \{(\Delta S_1)^2 + 4|\beta|^2[|\alpha|^2 + |\gamma K|^2 \\ &\quad + 2 \operatorname{Re}(\alpha \gamma^* K^*)]\}^{1/2}. \end{aligned} \quad (\text{C1})$$

Now the K factor contributing to plasmon-induced modulation has the opposite sign compared to Eq. (11) of the main text. Consequently, the constructive interference ($-K$) increases the magnitude of the PB phase while destructive interference ($+K$) decreases it. The overall calculated PB phases ($|\Phi_{\text{PB}}| \approx 0.80\pi$, $|\Phi_{\text{PB}}| \approx 0.71\pi$) are larger but the plasmon-induced modulations are comparable to the previous case.

-
- [1] A. Shapere and F. Wilczek, *Geometric Phases in Physics* (World Scientific, Singapore, 1989).
 - [2] E. Cohen, H. Larocque, F. Bouchard, F. Nejadstari, Y. Gefen, and E. Karimi, Geometric phase from Aharonov–Bohm to Pancharatnam–Berry and beyond, *Nat. Rev. Phys.* **1**, 437 (2019).
 - [3] J. von Bergmann and H. von Bergmann, Focault pendulum through basic geometry, *Am. J. Phys.* **75**, 888 (2007).
 - [4] S. Pancharatnam, Generalized theory of interference and its applications, *Proc. Indian Acad. Sci. A* **44**, 247 (1956).
 - [5] C. Brosseau, *Fundamentals of Polarized Light* (Wiley, New York, 1998).
 - [6] M. V. Berry, Quantal phase factors accompanying adiabatic changes, *Proc. R. Soc. Lond. A* **392**, 45 (1984).
 - [7] Y. Aharonov and D. Bohm, Significance of electromagnetic potentials in the quantum theory, *Phys. Rev.* **115**, 485 (1959).
 - [8] M. Born and E. Wolf, *Principles of Optics* (Cambridge University Press, Cambridge, 2019).
 - [9] M. Amniet-Talab and H. Rangani Jahromi, Design of geometric phase gates and controlling the dynamic phase for a two-qubit Ising model in magnetic fields, *Proc. R. Soc. A* **469**, 20120743 (2013).
 - [10] T. van Dijk, H. F. Schouten, W. Ubachs, and T. D. Visser, The Pancharatnam–Berry phase for noncyclic polarization changes, *Opt. Express* **18**, 10796 (2010).
 - [11] S. Daniel, K. Saastamoinen, T. Saastamoinen, I. Vartiainen, A. T. Friberg, and T. D. Visser, Surface plasmons carry

- the Pancharatnam–Berry geometric phase, *Phys. Rev. Lett.* **119**, 253901 (2017).
- [12] F. De Zela, in *Theoretical Concepts of Quantum Mechanics*, edited by M. R. Pahlavani (InTech, Rijeka, 2012), Chap. 14.
- [13] L. Garza-Soto, N. Hagen, D. Lopez-Mago, and Y. Otani, Wave description of geometric phase, *J. Opt. Soc. Am. A* **40**, 388 (2023).
- [14] A. Hannonen, H. Partanen, J. Tervo, T. Setälä, and A. T. Friberg, Pancharatnam–Berry phase in electromagnetic double-pinhole interference, *Phys. Rev. A* **99**, 053826 (2019).
- [15] A. Hannonen, H. Partanen, A. Leinonen, J. Heikkinen, T. K. Hakala, A. T. Friberg, and T. Setälä, Measurement of the Pancharatnam–Berry phase in two-beam interference, *Optica* **7**, 1435 (2020).
- [16] A. Leinonen, A. Hannonen, H. Partanen, J. Heikkinen, T. Setälä, A. T. Friberg, and T. Hakala, Non-cyclic continuous Pancharatnam–Berry phase in dual-beam interference, *Commun. Phys.* **6**, 132 (2023).
- [17] H. Raether, *Surface Plasmons on Smooth and Rough Surfaces and on Gratings* (Springer, Berlin, 1988).
- [18] S. A. Maier, *Plasmonics: Fundamentals and Applications* (Springer, New York, 2007).
- [19] H. F. Schouten, N. Kuzmin, G. Dubois, T. D. Visser, G. Gbur, P. F. A. Alkemade, H. Blok, G. W. 't Hooft, D. Lenstra, and E. R. Eliel, Plasmon-assisted two-slit transmission: Young's experiment revisited, *Phys. Rev. Lett.* **94**, 053901 (2005).
- [20] A. Leinonen, K. Saastamoinen, H. Pesonen, G. Wu, T. D. Visser, J. Turunen, and A. T. Friberg, Polarization modulation by surface plasmons in Young's double-slit setup, *Phys. Rev. A* **104**, 043503 (2021).
- [21] A. Leinonen, H. Pesonen, T. D. Visser, J. Turunen, and A. T. Friberg, Plasmon echoes and polarization dynamics in Young's double-slit setup, *Phys. Rev. A* **106**, 063519 (2022).
- [22] R. C. Weast, *CRC Handbook of Chemistry and Physics* (CRC Press, Boca Raton, FL, 1983), 64th ed.
- [23] H. Kim, J. Park, and B. Lee, *Fourier Modal Method and its Applications in Computational Nanophotonics* (CRC Press, Boca Raton, FL, 2017).
- [24] L. Mandel and E. Wolf, *Optical Coherence and Quantum Optics* (Cambridge University Press, Cambridge, 1995).
- [25] J. W. Goodman, in *Introduction to Fourier Optics* (Roberts & Company, Greenwood Village, CO, 2005), 3rd ed., p. 52.
- [26] S. Divitt, M. Frimmer, T. D. Visser, and L. Novotny, Modulation of optical spatial coherence by surface plasmon polaritons, *Opt. Lett.* **41**, 3094 (2016).
- [27] A. Arbabi, Y. Horie, M. Bagheri, and A. Faraon, Dielectric metasurfaces for complete control of phase and polarization with subwavelength spatial resolution and high transmission, *Nat. Nanotechnol.* **10**, 937 (2015).
- [28] C. P. Jisha, S. Nolte, and A. Alberucci, Geometric phase in optics: from wavefront manipulation to waveguiding, *Laser Photonics Rev.* **15**, 2100003 (2021).
- [29] Y. Guo, M. Pu, Z. Zhao, Y. Wang, J. Jin, P. Gao, X. Li, X. Ma, and X. Luo, Merging geometric phase and plasmon retardation phase in continuously shaped metasurfaces for arbitrary orbital angular momentum generation, *ACS Photonics* **3**, 2022 (2022).